All-fibered coherent-differential absorption lidar at 1.645 μm for simultaneous methane and wind-speed measurements

Simon Le Méhauté, Philippe Benoit, Nicolas Cézard, Didier Goular, Christophe Planchat, Matthieu Valla, Agnes Dolfi-Bouteyre, Xavier Watremez, Hervé Delbarre

All-fibered coherent Differential Absorption Lidar at 1.645 μm for simultaneous methane and wind-speed measurements

Simon Le Méhauté[a], Philippe Benoit[a], Nicolas Cézard[a], Didier Goular[a], Christophe Planchat[a], Matthieu Valla[a], Agnès Dolfi-Bouteyre[a], Xavier Watremez[b], and Hervé Delbarre[c]

[a]ONERA, The French Aerospace Lab, FR-91123 Palaiseau Cedex, France
[b]Total E&P, CST-JF, Avenue Larribau, FR-64018 Pau Cedex, France
[c]Laboratoire de Physico-Chimie de l'Atmosphère (LPCA), Université du Littoral Côte d'Opale, 59140 Dunkerque, France

ABSTRACT

Here we report on the development of a new coherent-DIAL system as well as first quantitative measurements of simultaneous gas mixing ratio and radial wind-speed with the instrument. Integrated measurement of atmospheric methane (CH_4) mixing ratio between the instrument and a hard-target located at 2.25 km has been conducted with a relative precision of nearly 20% in 17 s. The measurement procedure also gives information on integrated water vapor (H_2O) mixing ratio.

Keywords: lidar, methane, wind, fiber laser, Raman amplifier

1. INTRODUCTION

Quantification of methane leaks and control of plume evolution in the vicinity of industrial sites is crucial for oil & gas companies, especially in the case of a major crisis event occurrence. A better control of such events would directly lead to (i) better decision-making and thus improved on-site security because of the explosive properties of methane (ii) financial losses estimations (iii) environmental impact quantification, methane being one of the major greenhouses gases. From the first point arises the need of remote-sensing because security protocols could lead to the implementation of a no-go area around the leak source hence making *in-situ* sensors unsuitable.

The majority of active CH_4 remote sensing systems one can find in the literature are TDLAS (Tunable Diode Laser Absorption Spectroscopy) sensors that give information at short range given the implementation of a retro-reflector or IP-DIAL (Integrated-Path Differential Absorption Lidar) system designed for spaceborne and airborne monitoring of methane. The latter developments being stimulated by the laucnh of MERLIN mission[1] by 2025. Last year, Amediek et. al[2] had demonstrated leak quantification with such an instrument, however wind information is provided by a nearby weather station.

In the context of a collaborative project (with french oil & gas company TOTAL) called NAOMI (New Advanced Observation Method Integration), ONERA is currently developing a demonstrator for all-fibered 1.645 μm coherent-DIAL lidar called VEGA ("VEnt & GAz" - french for "Wind & Gas"). A coherent-DIAL system operating at 2 μm has already been demonstrated for CO_2 measurement but with a solid-state laser and a free space architecture[3]. As stated,VEGA has been designed with the objective of characterizing CH_4 leaks terms of emission rate, hence measuring simultaneously gas mixing ratio and wind-speed inside a gas plume with adequate spatio-temporal resolution. The choice of optical fiber technology make our system alignment free, robust and compact thus suitable for deployment on the ground.

2. SYSTEM CONFIGURATION

This section discusses the lidar design (2.1), laser system physics and obtained performances (2.2) as well as wavelength sequencing for DIAL measurement (2.3).

Further author information: (Send correspondence to S. Le Méhauté)
E-mail: simon.lemehaute@onera.fr, Telephone: +33 (0)1 80 38 63 51

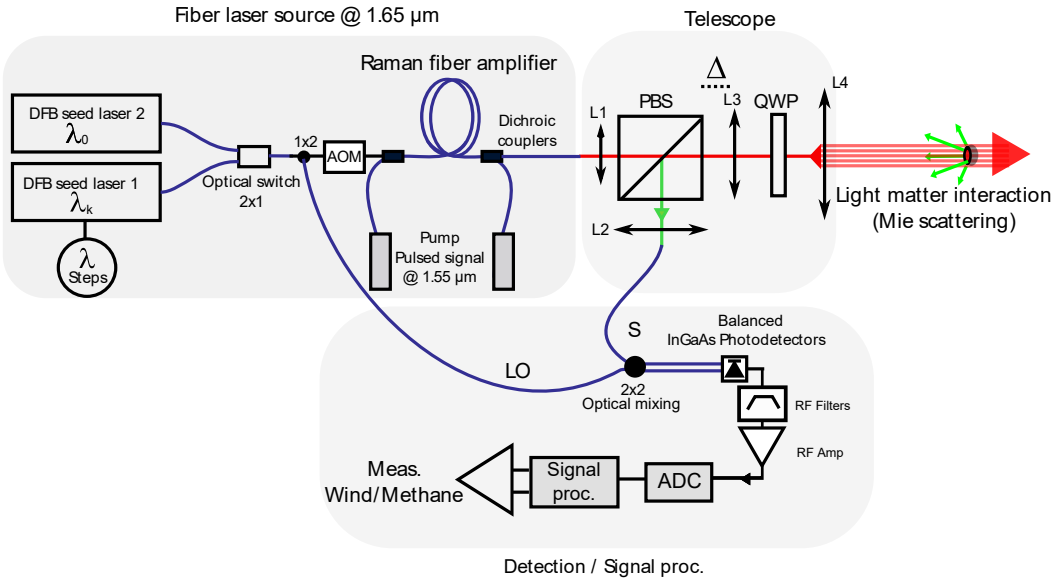

FIGURE 1. Instrumental setup for VEGA lidar

2.1 Overall lidar design

As depicted in Fig. 1, the lidar relies on a fiber laser system consisting of a Master Oscillator Fiber Power Amplifier (MOFPA) configuration alternatively seeded by two DFB (Distributed FeedBack) laser diodes emitting a few mW in CW operation around $1.645\,\mu m$. A first part of this CW signal provides a phase reference, local oscillator (LO) for coherent detection. LO power is set close to $1mW$ to ensure a shot-noise limited detection. The remaining part experiences a $80MHz$ frequency-shift through an Acousto Optic Modulator (AOM) and enters the amplifier. This shift ensures both wind-speed sign disambiguation and allows to avoid electronics $1/f$ noise. After amplification, the system emits linearly polarized optical pulses of several μJ in the $1.645\,\mu m$ region with a high repetition rate of $20\,kHz$. More detailled performances of the laser system will be discussed in Section 2.2.3.

After expansion through the telescope ($L1-4$) the beam has a radius of $3\,cm$ and is sent to the atmosphere through an exit lens of $5\,cm$ diameter. Backscattering signal arising from the target or Mie scattering on particles (S) is collected through the same telescope (monostatic configuration). The combination of a quarter wave plate (QWP) and a polarizaton beam splitter (PBS) allows to separate emission (red) and reception (green) channels. Once collected, the signal (S) is coupled into an optical fiber and sent to a balanced $InGaAs$ photo-detectors where it interferes with the LO. The generated RF beatnote signal oscillates at intermediate frequency (IF) $f_0 \pm f_d$, f_d being the Doppler shift. Signal and noise are then amplified and filtered around this frequency before being digitized in time domain at sample frequency $250MHz$ with an Analog to Digital Converter (ADC). Overall lidar design as well as obtained laser performances are summarized in Table 1. Further signal processing steps will be discuss in Section 3.

2.2 Pulsed fiber laser

The system is taking advantage of a specially designed Raman fiber amplifier. The latter has the ability to provides optical gain in a spectral region of interest for CH_4 measurement in near infra-red region. Two needs emerge for laser system specifications (i) obtaining enough gain from the amplifier in the $1.645\,\mu m$ region to meet the requirements of CH_4 DIAL measurement (ii) having adequate spectral linewidth and polarization state for coherent detection (hence the amplifier is qualified as "single frequency").[4]

2.2.1 Stimulated optical scattering

Although effects due to non linearities inside optical fiber may set the upper limit for the emitted power of a given system, these phenomenons are also often used for frequency conversion. Considering that commonly used

rare-earth doped amplifiers such as EDFA (Erbium Doped Fiber Amplifier) do not provide sufficient optical gain in the spectral region of interest, our laser system relies on frequency conversion arising from Stimulated Raman Scattering (SRS) during the propagation. SRS is a third-order incoherent process in which energy transfer occurs between two electric fields of respective frequency f (pump) and $f - \Delta f_R$ (signal) through coupling with optical phonons (of frequency Δf_R) inside a material. For SiO_2 molecules composing an optical fiber, the frequency shift Δf_R is known to be close to $13\,THz$ (corresponding to $0.1\,\mu m$ around $1.5\,\mu m$). Due to optical phonons short lifetime SRS is a relative broadband effect with a typical width of $2\,THz$. Thus one can both (i) amplify a seed signal at $1.645\,\mu m$ by pumping a silica fiber at $1.545\,\mu m$, a wavelength which allows the implementation of widely developed telecommunications components, including high-power amplifiers, modulators, etc.. (ii) tune the emission wavelength of the seed over an interesting spectral range and still observing optical gain. VEGA's laser system relies on this effect in a pulsed regime to meet peak power requirements for the pump and thus for lidar measurements.

This system uses a HNLF (Highly Non Linear Fiber) to improve SRS efficiency. In practice, in terms of energy ouput, the main limitation of a single frequency Raman amplifier is due to the relatively high threshold of SRS in comparison to another non-linear scattering process occurring inside optical fiber : Simulated Brillouin Scattering (SBS). This phenomena occurs for both pump and signal. In terms of physical concepts, it is similar to SRS although frequency shift and gain bandwidth are shown to be of different orders of magnitude (respectively $11GHz$ and a few tens of MHz). Such a difference can be explained by the nature of the coupling : an acousto-optical interaction involving phonons with lower frequency and higher lifetimes. One can uses these distinctions between the two stimulated optical scattering processes to implement SBS mitigations techniques (either passive or active) that do not affect SRS. Such techniques allow to balance the efficiency of the two processes. Since there is no requirement on the temporal coherence of the pump source, spectral broadening techniques can be used to significantly increase SBS threshold. As far as the $1.645\,\mu m$ signal is concerned, any spectral broadening would directly reduce lidar performances. That is why passive SBS mitigation technique, such as the application of a longitudinally dependant constraint on the HNLF, is chosen.

2.2.2 Non-linear phase term

As mentioned, one must avoid any spectral broadening of the signal during its amplification. However such a broadening may occur in the HNLF due to Cross Phase Modulation (XPM) between the high peak power pump and the signal. Considering equations describing both XPM and SRS, one can derive the following expression.[5] It states the signal experiences a phase evolution $\varphi_{NL}(t)$ proportional to the logarithm of the optical gain $G(t)$:

$$\varphi_{NL}(t) = k \times ln\Big(G(t)\Big) \tag{1}$$

By using a square shaped pulse for the pump, the phase shift added by XPM to the amplified signal is constant and thus no spectral broadening is induced.

2.2.3 Obtained performances

In the end, the implementation of the different techniques presented in 2.2.1 and 2.2.2 allow the designed laser system to deliver linearly polarized optical pulses of $100\,ns$ time width. An output energy of $12\mu J$ exiting a monomode fiber has been demonstrated. Optical fiber has a large surface to volume ratio which allows better heat dissipation and thus high pulse repetition rate (PRF), namely $20\,kHz$ in our case. Despite the non linear effects that can occurs during the propagation inside the optical fiber and the non-linear nature of the amplification process itself, generated pulses have been measured to be nearly Fourier-transform limited with a typical width of $10MHz$ (Fig. 2).

When it comes to wind-speed estimation, an important parameter is the stability of the laser spectrum first order moment f_0 (or barycentre) because this frequency acts as a reference for Doppler measurement. In the $1.6\,\mu m$ region the Doppler shift is close to $1MHz/(m.s^{-1})$, so any uncertainty on this quantity hence has a significant impact on the quality of wind speed estimates. This stability has to be studied for typical accumulation time for Doppler measurement τ. This has been characterized measuring the Allan deviation of barycentre (Fig. 3). The results show the laser-induced error made on Doppler-shift is less than $0.1\,MHz$ over accumulation time between $10\,ms$ and $100\,s$

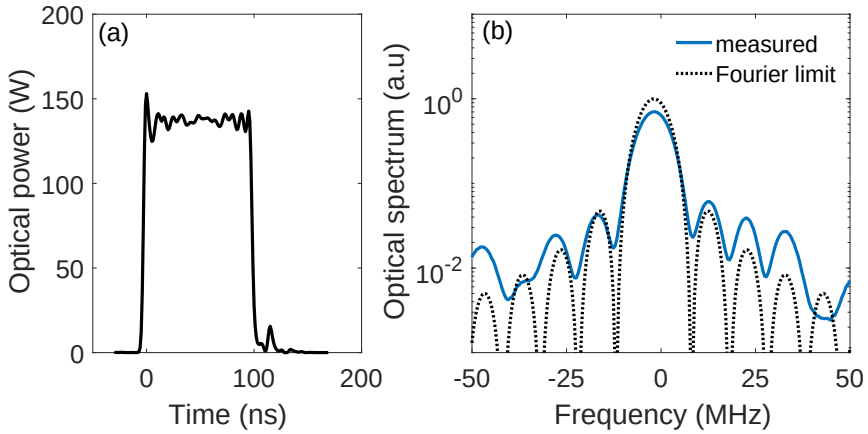

FIGURE 2. (a) Square optical pulse emitted by the laser (b) Optical spectrum obtained from heterodyne measurement.

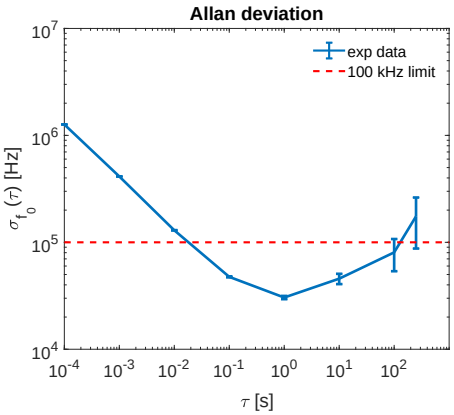

FIGURE 3. Allan deviation of the first order moment of laser emission spectrum. Laser-induced error on wind speed measurement is less than $\simeq 0.1 m.s^{-1}$ for accumulation time between $10\,ms$ and $100\,s$.

2.3 Measurement sequence

Taking advantage of the versatily of telecommunications components and the properties of laser diodes, one can tune the emitted wavelength of the DFB through injection current and/or temperature. Assuming a linear evolution the of emitted wavelength with current, the tuning coefficient has been measured to be close to $700 MHz/mA$ and the absolute wavelength has been calibrated with a CH_4 cell filled at atmospheric pressure. Such an order of magnitude ensures both a high spectral resolution across the chosen absorption line of CH_4 at atmospheric pressure (typical width $4\,GHz$) and also an interesting frequency excursion in spectral region in which water vapor signature can also be observed. Thus, DFB_1 will be modulated with injection current to generate a sequence of wavelengths λ_k across methane and water-vapor absorption lines while DFB_2 will provide a fixed reference wavelength λ_0.

As depicted in Fig. 4, the sequence is the following : an optical switch (OS) alternates between λ_1 and λ_0 at frequency $f_{01} = 2Hz$ and these wavelengths do not evolve during time $\tau_s = 60\,s$ after which a current step is applied to DFB_1. The same process is repeated for λ_2 and λ_0 etc..

λ_k are often referred as *on-line* wavelengths while λ_0 is referred as *off-line*. Because the emitted wavelengths are very close, it is assumed that propagation of any λ_k through the atmosphere only differs from λ_0 because of molecular absorption (either CH_4 or H_2O). This is the principle on which DIAL technique is based. Thus, normalizing any *on-line* estimated return signal with *off-line* signal, eliminates every other atmosphere (or target) parameters which governs the magnitude of this signal such as backscatterring coefficient, losses due

to scatterring, etc. Of course this assumes these parameters are stationary within the time scale between the emission of λ_k and λ_0 (which is $1/f_{01} = 500ms$ in our case).

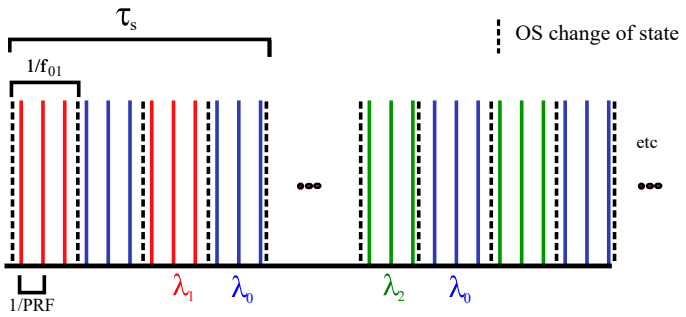

FIGURE 4. Schematic of wavelength sequencing for IP-DIAL measurement of methane and water vapor with VEGA. OS : optical switch, f_{01} is switch frequency, τ_s is accumulation time for one wavelength pair in the sequence and PRF is the pulse repetition frequency of the laser

TABLE 1. Summary of lidar configuration and laser source performances

LIDAR CONFIGURATION

Quantity	**Value**	**Notes**
Exit lens diameter	$5cm$	Monostatic configuration
Beam radius on exit lens diamter	$3cm$	
Detection	$InGaAs$ detectors	
Intermediate frequency	$80\,MHz$	Provided by the AOM
LO power	$1\,mW$	
ADC sampling frequency	$250MHz$	

LASER PERFORMANCES

Quantity	**Obtained**	**Notes**
Output energy	$12\mu J$	Brillouin limited
Temporal width	$100\,ns$	Pulseshape : square, $15m$ resolution
Spectral width	$10\,MHz$	Fourier-transform limited
Stability of IF	$\leq 0.1MHz$	for τ between $10ms$ and $100s$
Pulse repetition frequency (PRF)	$20\,kHz$	-
Wavelength tunability	$0.5\,nm$	Around $1.6545\mu m$ - limited by a filter
Polarization	Linear	-
Beam quality factor M^2	Close to 1	Monomode fiber output
Switch frequency f_{01}	$2Hz$	-

3. SIGNAL PROCESSING AND PARAMETERS RETRIEVAL

Once digitized, a sliding gate is applied to time domain lidar data, dividing that signal in smaller parts referred as range gates (RG). The width of these gates gives the lidar longitudinal resolution, thus its lower limit can be written as $c\tau_{pulse}/2$, τ_{pulse} being the temporal pulse width. Then Power Spectral Density (PSD) is computed for each RG, accumulated over time f_{01}^{-1} and normalized by the noise PSD (Fig. 5). One can apply zero-padding on time domain data to enhance the spectral resolution for PSD calculation. Accumulated and normalized PSD S_τ carries all the needed information for lidar measurement : (i) optical flux scattered from the hard-target is the zero-order moment inside a given bandwidth B around its maximum at that distance and (ii)

the range resolved Doppler-shift f_d corresponding to first order moments f_1, relatively to IF f_0. This section will discuss the physical meaning of these moments and their estimations as well as mixing ratios estimates.

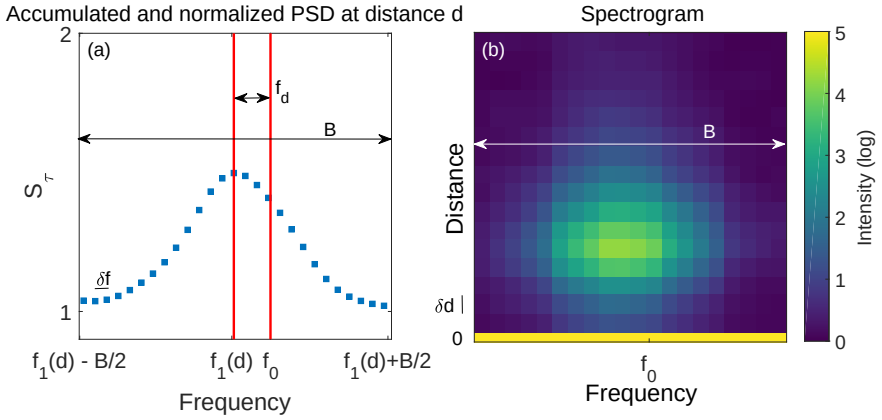

FIGURE 5. (a) Accumulated and normalized PSD $S_\tau(f)$ for one RG at distance d depicted inside detection bandwidth B (b) The representation with respect to distance -each RG is displayed- and frequency is often referred as "accumulated spectrogram" (simulations results)

3.1 Carrier to noise ratio estimation

Useful lidar time domain signal, called heterodyne current, consists of interferences between backscattered and reference optical fields and can be written as proportional to their products. Because of the presence of noise current, the total lidar signal can be written as the sum of heterodyne and noise current. One commonly used lidar performanced indicator is the so called Carrier to Noise Ratio (CNR) which consists of heterodyne current power normalized by noise current power. Because both heterodyne and noise current have a zero mean, the CNR is defined as follow :

$$CNR = \frac{\sigma^2_{i_h}}{\sigma^2_{i_b}} \tag{2}$$

However, it is important to recall that, not only noise, but also heterodyne current have a random nature. Because of their position inside the illuminated volume, each of particle scatters a part of the incident field with random phase. The total backscattered optical field consists of the sum of these "elementary" fields and thus, is also random by nature. This phenomenon is called speckle noise. As already mentioned, one common way of estimating CNR is by computing the zero-order moment of normalized PSD in the detection bandwidth B. This bandwidth is set to $30MHz$ as it must contain all the energy :

$$\hat{CNR}(d) = \frac{1}{B}\int_B S_\tau(d,f)df - 1 \tag{3}$$

3.2 Radial wind speed

Because of their dimensions and weight, aerosols scatters IR light in the so called Mie scattering regime and are also good tracers of wind-speed. They evolve in the atmosphere following wind field with little velocity dispersion. Hence, one can measure the induced Doppler-shift on backscattered laser signal to measure range-resolved radial wind speed v_r. The following estimate will be used; it consists of barycentre of the PSD around its maximum :

$$\hat{v}_r(d) = -\frac{1}{2}\lambda \times \left[\frac{\int f \times S_\tau(d,f)df}{\int S_\tau(d,f)df} - f_0\right] \tag{4}$$

3.3 Gases mixing ratios : IP-DIAL measurement

The goal here is to estimate CH_4 and H_2O average mixing ratios between the lidar and a hard target located at distance L from obtained data. Such a technique is called IP-DIAL (Integrated-Path DIAL).

As discussed, heterodyne current is proportional to the product of LO and backscattered optical field. Hence, CNR is proportional to backscattered optical flux and a ratio of CNR at different wavelengths is proportional to $e^{-2\Delta OD(\lambda_k,\lambda_0,L)}$ according to Beer-Lambert's law, OD being the optical depth. Such a ratio thus gives information on molecular absorption. Wavelength sequencing allows to obtain information on both methane and water vapor mixing ratios (ppm), respectively x_1 and x_2. A linear model for these quantities can be written in the following form :

$$-\frac{1}{2}log\Big(\frac{\epsilon(\lambda_k)^{-1}CNR(\lambda_k,L)}{\epsilon(\lambda_0)^{-1}CNR(\lambda_0,L)}\Big) = x_1\int_0^L WF_1(\lambda_k,z)dz + x_2\int_0^L WF_2(\lambda_k,z)dz \tag{5}$$

With ϵ being the emitted energy which varies with injection current. The weight functions WF are the differential absorption cross-sections hence $\Big[\sigma(\lambda_k,z)-\sigma(\lambda_0,z)\Big]$. Here, the approximation of considering a constant differential cross-section along the horizontal line of sight has been made. These cross-sections have been calculated using HITRAN2012 spectral database.

$$\int_0^L WF_i(\lambda_k,z)dz \simeq \Delta\sigma_i(\lambda_k,\lambda_0)\Delta z \tag{6}$$

By estimating the following quantity, one can perform a linear least-square optimization with the model of Eq. 5 to estimate x_1 and x_2. If one **has** either enough realizations of each $\hat{Y}_k$ to estimate its empirical variance, or a theoritical expression of it, the fit procedure can be refined and the estimation error can also be calculated.

$$\hat{Y}_k = -\frac{1}{2}log\Big(\frac{\epsilon(\lambda_k)^{-1}C\hat{N}R(\lambda_k,L)}{\epsilon(\lambda_0)^{-1}C\hat{N}R(\lambda_0,L)}\Big) \tag{7}$$

4. RESULTS & DISCUSSION

To obtain the results below the lidar configuration is that of Section 2 and laser beam is focused at $150\,m$. It points to a telecommunication antenna. The distance between the instrument and this target is $2.25\,km$, its signature can be observed in Fig. 7a. RG corresponding to $30\,m$ has been applied to time domain signal. The sequencing procedure described in Section 2.3 has been used with 17 wavelengths λ_k and the reference wavelength λ_0 depicted in Fig. 6, sharing typical OD for both methane and water vapor. Accumulation time for a fixed couple of wavelengths $[\lambda_k,\lambda_0]$ is set to $\tau_s = 60\,s$ while the two wavelengths alternates every $1/f_{01} = 500\,ms$.

The temporal interval between two successive estimations of $C\hat{N}R$ and $\hat{v}_r$ is also $500\,ms$. As each $\hat{Y}_k$ necessitates $C\hat{N}R$ for λ_k and λ_0, they are estimated every second. At the end of the $17min$ measurement, each quantity has been estimated 60 times. Such statistical samples allow to measure mean range-resolved radial wind-speed and its associated empiric error for a $500\,ms$ measurement. Results are depicted in Fig. 7b. The error is maintained below $1\,m.s^{-1}$ up to $300\,m$ range. Fig. 7c presents IP-DIAL measurements perfomed with VEGA for both gases. The spectral signature is clearly observable and the estimation algorithm returns a concentration of methane of $2.3\pm0.51\,ppm$ and a concentration of water vapor of $27000\pm9800\,ppm$. The relative random error are respectively 22% and 36%. Performing a least-square estimation optimization on Y_k in order to estimate x_1 and x_2 need the whole $17\,\lambda_k$ to be emitted, hence the results and error bars are given for a accumulation time of $17\,s$. The obtained order of magnitude are in agreement with the expectations for atmospheric levels of methane and water vapor. A better wavelength calibration procedure could significantly improve this measurement, especially for water vapor. Time accumulation could also be used, though speckle from the hard-target may have coherence time longer that the PRF.

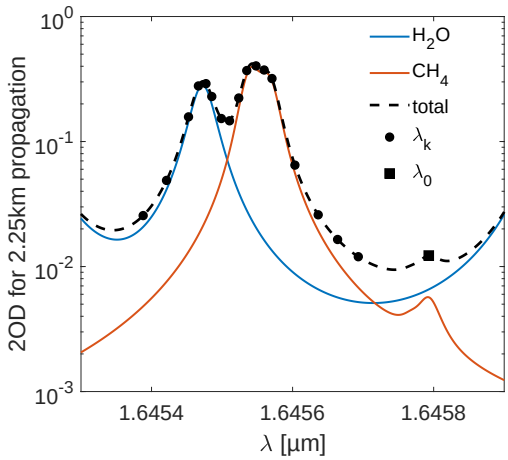

FIGURE 6. Two ways optical depth $2OD$ for $2.25km$ propagation with methane and water vapor concentration being respectively 1.8 and 20×10^3 ppm and an example of wavelength sequence for DIAL measurement with $17\lambda_k$. Absorption cross-sections are calculated using HITRAN2012 database

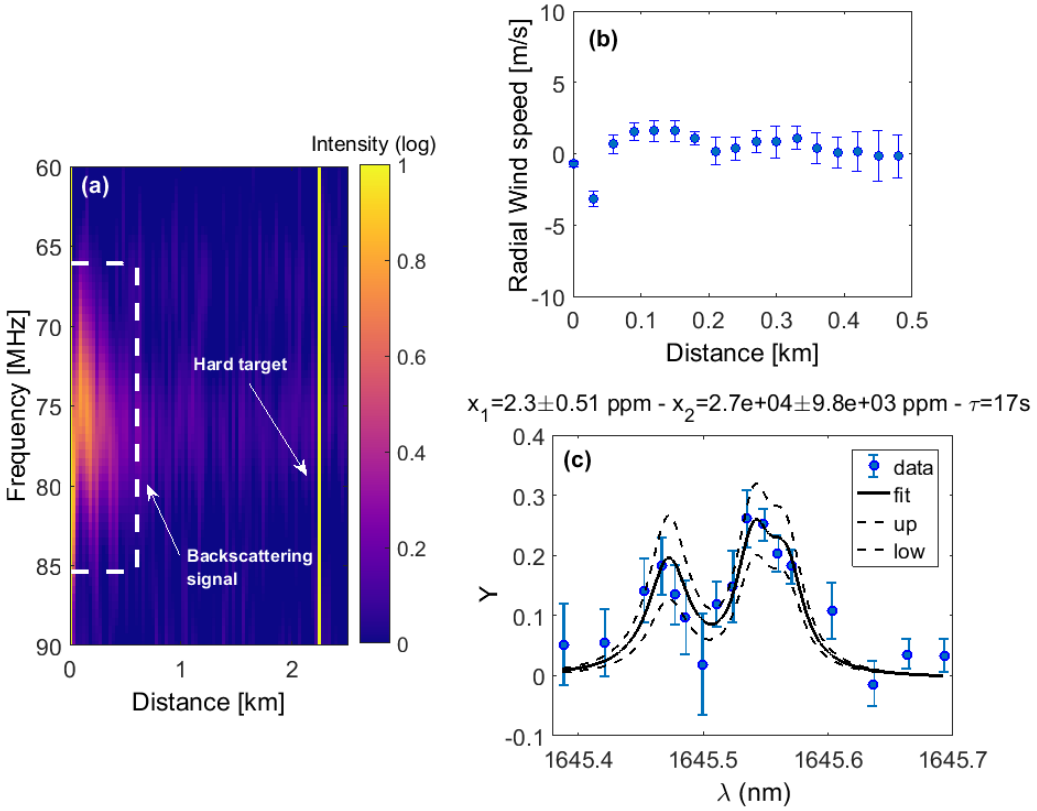

FIGURE 7. (a) Accumulated and normalized lidar signal spectrogram along the LOS for accumulation time of $500\,ms$ (b) Range-resolved radial wind speed retrieval measuring Doppler shift on observed Mie backscattering signal and associated error for $500\,ms$ measurement time(c) Gases mixing ratio retrieval with lidar data performing linear least-square optimization and associated error on $\tau = 17s$ measurement time. Random relative error are estimated to 22% and 36% respectively for methane and water vapor

5. CONCLUSION

We have demonstrated a coherent-DIAL system capable of simultaneous estimations of range resolved wind speed measurement and integrated mixing ratio of methane and water vapor. It is based on Doppler lidar architecture with a newly designed fiber laser amplifier that relies on Raman scattering to provide both optical gain in a region of absorption of methane and suitable performances for its implementation as part of a heterodyne lidar. Using a sequence of wavelengths allowed us to perform IP-DIAL measurement of ambient level CH_4 and H_2O with a relative error of respectively 22 and 36% in $17s$. This is to our knowledge the first CH_4 measurement with a coherent-DIAL system. These results constitute a step towards a system able to characterize leak rate of fugitive CH_4 emissions in the field.

ACKNOWLEDGMENTS

This work was funded by Total $E\&P$ and ONERA partnership under NAOMI contract.

REFERENCES

[1] Pierangelo, C., Millet, B., Esteve, F., Alpers, M., Ehret, G., Flamant, P., Berthier, S., Gibert, F., Chomette, O., Edouart, D., et al., "Merlin (methane remote sensing lidar mission) : An overview," in [*EPJ Web of Conferences*], **119**, 26001, EDP Sciences (2016).

[2] Amediek, A. et al., "CHARM-F a new airborne integrated-path differential-absorption lidar for carbon dioxide and methane observations : measurement performance and quantification of strong point source emissions," *Applied Optics* **56**, 5182 (jun 2017).

[3] Gibert, F., Flamant, P. H., Bruneau, D., and Loth, C., "Two-micrometer heterodyne differential absorption lidar measurements of the atmospheric CO_2 mixing ratio in the boundary layer," *Applied Optics* **45**, 4448 (jun 2006).

[4] Cézard, N., Benoit, P., and Canat, G., "1.6 micron fiber laser source for CH_4 gas leak detection," *EPJ Web of Conferences* **119**, 05010 (2016).

[5] Benoit, P., Cézard, N., Mussot, A., Kudlinski, A., and Canat, G., "Nonlinear phase added by a raman fiber amplifier to a single-frequency seed laser," in [*CLEO : Science and Innovations*], SW4P–4, Optical Society of America (2016).